An Ankle-Foot Prosthesis for Rock Climbing Augmentation

Emily A. Rogers, *Graduate Student Member, IEEE*, Matthew E. Carney, Seong Ho Yeon, *Graduate Student Member, IEEE*, Tyler R. Clites, Dana Solav, *Member, IEEE*, and Hugh M. Herr, *Member, IEEE*

***Abstract*— This research presents the design and preliminary evaluation of an electromyographically (EMG) controlled 2-degree-of-freedom (DOF) ankle-foot prosthesis designed to enhance rock climbing ability in persons with transtibial amputation. The prosthesis comprises motorized ankle and subtalar joints, and is capable of emulating some key biomechanical behaviors exhibited by the ankle-foot complex during rock climbing maneuvers. The free space motion of the device is volitionally controlled via input from EMG surface electrodes embedded in a custom silicone liner worn on the residual limb. The device range of motion is 0.29 radians of each dorsiflexion and plantar flexion, and 0.39 radians each of inversion and eversion. Preliminary evaluation of the device was conducted, validating the system mass of 1292 grams, build height of 250 mm, joint velocity of 2.18 radians/second, settling time of 120 milliseconds, and steady state error of 0.008 radians. Clinical evaluation of the device was performed during a preliminary study with one subject with transtibial amputation. Joint angles of the ankle-foot, knee, and hip were measured during rock climbing with the robotic prosthesis and with a traditional passive prosthesis. We found that the robotic prosthesis increases the range of achieved ankle and subtalar positions compared to a standard passive prosthesis. In addition, maximum knee flexion and hip flexion angles are decreased while climbing with the robotic prosthesis. These results suggest that a lightweight, actuated, 2-DOF EMG-controlled robotic ankle-foot prosthesis can improve ankle and subtalar range of motion and climbing biomechanical function.**

***Index Terms*— Assistive technology, biomechatronics, prosthesis design, quasi-passive, rehabilitation robotics, wearable robots.**

I. Introduction

CURRENT lower extremity prosthesis research and development largely focus on the design and control of devices to increase mobility and improve function during activities of daily living such as level ground walking and navigating stairs and ramps. State of the art robotic prostheses allow persons with lower limb amputation to walk over level ground with gait patterns similar to those of people with intact biological limbs [1]. However, these prostheses do not allow users to efficiently and comfortably perform other recreational and athletic activities. Physical activity has a positive effect on physical and psychological health, but participation in sports and physical activities decreases by an average of 86% following lower limb amputation [2]. For many individuals with lower extremity amputation, their prosthesis technology is a barrier to participation in sports [3]. Despite advances in rehabilitation technology and prosthesis design, only 40% of persons with physical impairment participate in regular sporting activities, compared to 73% of the general population [4], [5]. There are numerous benefits of participation in athletics, including: exercise endurance, strength, cardiovascular health, balance, motor skills, improved self image, body awareness, motor development, mood, decreased cardiac risk factors, and improved proficiency in the use of prostheses [4]. One sport which has greatly increased in popularity in recent years is rock climbing [6]. In addition, rock climbing has been shown to be beneficial for the rehabilitation of people with lower limb amputations [6]. However, current lower extremity prostheses lack functionality necessary to fully restore climbing function.

In order to understand the unique requirements of a prosthesis designed to be used while rock climbing, a brief overview of the the biomechanics of rock climbing is presented. Biomechanical research on rock climbing shows foot orientation while climbing is critical to control balance, decrease energetic cost of reaching moves with the upper body, and to orient the body such that the center of mass is closer to the wall [7]. Studies show that elite climbers use a wide variety of foot and ankle positions during climbing, including edging with 11 different types of foot positions while climbing, including edging with the inside or outside of the foot, toe contact, heel contact, flagging, and smearing [7]. There is more variety of foot positions than hand positions, and elite climbers employ a wider variety of foot positions while climbing than novice climbers [7]. This research indicates that varying position of both the ankle and subtalar joints while climbing is important for elite performance. In addition, experienced climbers demonstrate technique knowledge that improves climbing performance by varying foot position.

Manuscript received November 19, 2019; revised May 16, 2020 and August 6, 2020; accepted October 18, 2020. Date of publication October 23, 2020; date of current version February 25, 2021. This work was supported in part by the National Science Foundation Graduate Research Fellowship under Grant 1122374 and in part by the Massachusetts Institute of Technology (MIT) Media Laboratory Consortia. *(Corresponding author: Hugh M. Herr.)*

Emily A. Rogers, Matthew E. Carney, Seong Ho Yeon, Dana Solav, and Hugh M. Herr are with the Center for Extreme Bionics, Massachusetts Institute of Technology, Cambridge, MA 02139 USA (e-mail: hherr@media.mit.edu).

Tyler R. Clites was with the Center for Extreme Bionics, Massachusetts Institute of Technology, Cambridge, MA 02139 USA. He is now with the Anatomics Laboratory, University of California at Los Angeles (UCLA), Los Angeles, CA 90095 USA.

Digital Object Identifier 10.1109/TNSRE.2020.3033474

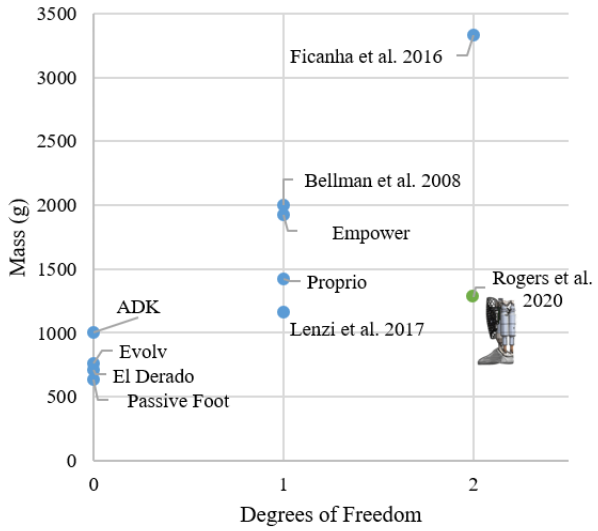

Fig. 1. Mass comparison with prior art. The novel 2-DOF prosthesis is lighter than any existing 2-DOF prostheses, and is comparable in mass with the lightest existing 1-DOF quasi-passive systems. [8]–[17].

Existing prostheses that may be useful for rock climbing include passive climbing-specific prostheses, quasi-passive devices, and powered ankle-foot walking prostheses. Climbing specific prostheses are limited to passive devices with no articulation about the ankle or subtalar joint. The El Dorado Z-axis foot [8], the Evolv adaptive foot [9], and the ADK Rock climbing foot [10] are commercially available devices that consist of a small passive foot with a fixed ankle position. These devices range in mass from 700 - 1000 grams (Fig. 1). A custom designed passive climbing prosthesis weighing 645 grams was used in this study, as it is the preferred device used by the subject for our study (Fig. 10). No climbing specific prosthesis exists that incorporates 2-degrees-of-freedom (DOF) with volitional control of position.

Powered prostheses are better able to match biological function by controlling joint position and torque during walking to more closely mimic biological function. The leader in powered ankle prosthesis technology is the Ottobock Empower [11]. This device injects power into the gait cycle to allow for powered plantar flexion during walking, allowing for walking gaits closer to that of individuals with intact biological limbs [12]. The Empower ankle weighs 1928 grams [11]. Another powered prosthesis matches ankle kinematics about 2-DOF [13]. This prototype device uses a cable driven system to control joint position and torque about the anle and subtalar axis. However, this device weighs 3000 grams [13]. Powered walking prostheses are able to adjust joint position and torque, however current devices are heavy and do not provide the user with volitional control of the device.

Quasi-passive prostheses are devices that use power to change joint position of the device but do not provide ankle torque during walking. These devices are lower mass than fully powered systems, due to lower torque and power requirements, and are able to provide many of the benefits of powered prostheses while utilizing lower mass and lower profile designs. One such device is the Ossur Proprio Foot [14], which automatically adjusts the swing phase ankle angle based on sensor values read by an on-board microcontroller, allowing the device to automatically adapt to terrain such as increasing the ankle dorsiflexion angle during stair ascent [15]. The Proprio foot weighs 1424 grams. Another device uses a ball screw transmission to change ankle position during swing. This device weighs 2000 grams and has 1-DOF of motion [16]. A similar device utilizes a non-backdrivable lead screw to drive the ankle through a cam, adjusting the ankle angle during the swing phase of walking [17]. This device weighs 1165 grams not including the foot and the battery. Due to the ability to decrease mass and power requirements, a quasi-passive design has potential to add utility to climbing, but existing devices only provide 1-DOF and are not volitionally controlled.

No device exists that allows for volitional control about 2-DOF. In addition, current powered devices are too heavy to be feasible for use while climbing (Fig. 1). Devices designed specifically for rock climbing do not allow for any range of motion at the ankle, or for volitional position control of the foot. Quasi-passive devices provide more functionality than passive, but still do not allow for volitional control of joint position. Powered prostheses are too heavy to be beneficial for use while climbing. In addition, none of the existing devices replicate biological function of the ankle-foot complex or provide volitional EMG control to provide the user with direct control over device motion.

This article presents the mechanical design and control of a novel lightweight, EMG controlled 2-DOF robotic ankle-prosthesis for rock climbing (Fig. 2), and preliminary device validation. The aim of this research is to assess the performance of this novel prosthesis design and to collect preliminary data on rock climbing performance in persons with transtibial amputation under volitional EMG control of a 2-DOF prosthesis. We hypothesize that a 2-DOF prosthesis that enables the climber to volitionally control ankle and subtalar joint position will improve climbing performance. A pilot study is conducted to evaluate biomechanics of a subject with unilateral transtibial amputation while rock climbing with the robotic prosthesis, and results are compared to biomechanics using with a traditional passive prosthesis. Joint angles of the hip, knee, and ankle-foot are measured, and joint torque about the prosthetic ankle and subtalar is recorded. Initial results from this pilot study demonstrate the potential to augment rock climbing in persons with amputation through the use of customized EMG-controlled mechatronic systems. This research will motivate future studies to assess the clinical efficacy of the prosthesis on a larger subject population.

II. Methods

This section describes the selection of design parameters, the mechanical, electrical, and controls design, and the evaluation methods.

Design parameters were developed for the prosthesis based on literature reviews and interviews with rock climbers with transtibial amputation (Table I). Design parameters for size

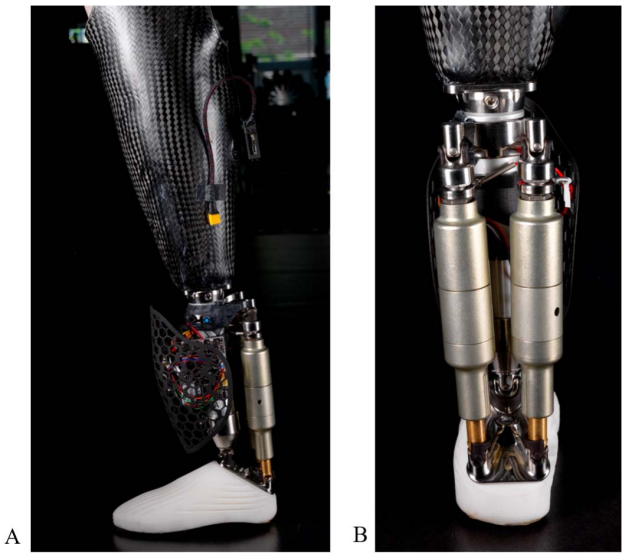

Fig. 2. Lateral view (A) and posterior view (B) of final rock climbing ankle-foot prosthesis.

TABLE I
DESIGN SPECIFICATIONS AND RESULTING PARAMETERS FOR ROBOTIC PROSTHESIS

Specification	Achieved Value
Range of Motion	Inversion/Eversion: ±0.39 radians Dorsiflexion/Plantar flexion: ±0.29 radians
Max Payload	100+ kg
Free-space torque	0.55 Nm
Velocity	2.18 radians/second
Accuracy	±0.008 radians
Mass	1292 g
Build height	250 mm
Battery life	> 4 hours

and mass of the system were determined based on the assumption that the prosthesis would account for 50% of the combined lower leg and foot length (femoral condyles to ground in neutral standing position), which was approximated as 14.25% body height, or 250 mm for a 50th percentile height male [18], [19]. The targeted mass was calculated based on anthropometric data for limb segment mass as a function of body mass, for a 75th percentile male (100 kg), with half of the lower leg and foot accounting for 3.05% of total body mass [19], [20].

Range of motion requirements were based off of static ankle range of motion for plantar flexion, dorsiflexion, inversion, and eversion [21]. Plantar flexion, inversion, and eversion range of motion requirements are set at less than biological levels in order to minimize build height of the system. Additional design requirements include user-controlled motion about the subtalar and ankle joint axes. The system must generate sufficient dynamic torque for free space motion of the foot while supporting a 100 kg user during stance. The device must move at a speed of 1 radian/second, with a free space positional accuracy of ± 0.008 radians. The battery life should be sufficient for a standard climbing session, or approximately 2 hours. Expected battery life was calculated based on the

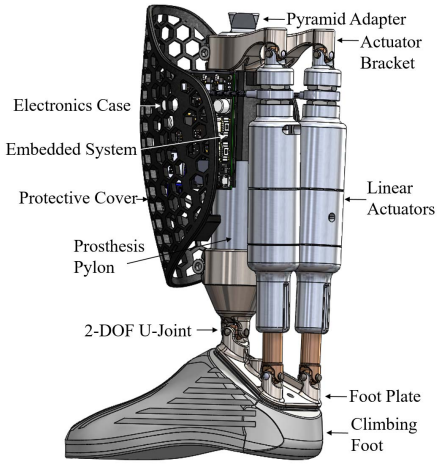

Fig. 3. Model of robotic climbing ankle showing subsystems of device: linear actuators, custom rock climbing foot, 2-DOF ankle U-joint, actuator mounting bracket, electronics, and protective cover.

energy consumption of the motors, sensors, and embedded system, and the assumption that the actuators will be utilized 50% of the time during a typical use session.

A. Mechanical Design

The described prosthesis is a quasi-passive device that allows for powered free-space position control with lower torque requirements than a dynamic actuator. The prosthesis utilizes a pair of non-backdrivable actuators, eliminating the need for dynamic torque output from the motors during stance and decreasing motor power requirements.

1) Ankle-Foot Prosthesis: The ankle-foot comprises two linear actuators, custom climbing foot, 2-DOF U-joint, actuator bracket, electronics, protective cover, prosthesis endoskeletal pylon, and pyramid adapter, as shown in Fig. 3.

The non-backdrivable custom linear actuators are described in detail in section II-A.2. A custom titanium mounting bracket, foot plate, and ankle joint attach to a standard prosthesis pylon to form the structure of the ankle-foot prosthesis. A custom rock climbing foot bolts onto the footplate, and an electronics case and protective cover attach to the pylon. The ankle and foot plate components form a 2-axis gimbal U-joint, forming the prosthetic ankle and subtalar joint. This joint allows the foot to plantar flex/dorsiflex, and invert/evert when driven by the actuators. The actuators are configured in a differential pair; when both actuators actuate in the same direction the ankle-foot prosthesis plantar flexes (Fig. 4A) or dorsiflexes (Fig. 4B). When one actuator contracts and the other extends, the device everts (Fig. 4C) or inverts (Fig. 4D). The U-joint consists of a custom foot plate and ankle joint attachment, with a bronze block in the center of the joint that dowel pins press into. This forms a secure connection with less than 0.03 mm of backlash in the joint, and can be disassembled and reassembled during maintenance or repairs.

The climbing foot was designed based on a 3D scan of a rock climbing shoe. The foot was designed to be approximately 60% the length of a 50th percentile male foot [19], as smaller feet allow climbers keep their center of mass closer

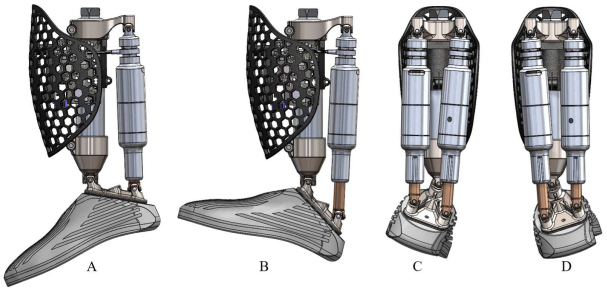

Fig. 4. The four major motions of the ankle-foot prosthesis: (a) plantar flexion occurs when both actuators contract, (b) dorsiflexion occurs when both actuators extend, (c) eversion occurs when the left actuator contracts and the right actuator extends, and (d) inversion when the left actuator extends and the right actuator contracts.

to the wall, and to precisely place their foot on small holds. The foot is manufactured using multijet fusion 3D printing (Proto Labs, Inc., Maple Plain, MN, USA) with nylon to allow for the complex geometry in a robust and lightweight package, and climbing shoe rubber is attached to the sole. The interface between the climbing foot and the foot plate is offset at a 0.52 radian angle, which maximizes the actuator height while reducing overall build height. A nylon electronics case attaches to the pylon to hold the lithium polymer (LiPo) battery, embedded system, and heat sink. A nylon protective cover attaches to the electronics case to protect the embedded system and analog signal and power wires. The mounting bracket, ankle, and foot plate are machined from 6AL-4V titanium. Total expected structural stiffness was calculated to determine expected deflection under load. The stiffness of the structural loop of the prosthesis is approximately 1.7×10^6 Newtons/meter, and the expected deflection under the under the worst case loading scenario is 1.2 mm at the toe. Maximum stress in all load bearing components was analyzed using FEA simulation software (Solidworks 2018, Dassault Systemes, Velizy-Villacoublay, France).

2) Linear Actuator Design: The linear actuator design is shown in Fig. 5. A brushed DC motor (DCX 22S, Maxon Group, Sachseln, Switzerland) drives an ACME thread lead screw (0.0625" lead), which in turn drives axial translation of the custom ACME nut. The screw is connected to the motor axle through a custom flexible shaft coupling (Helical Products Co., Santa Maria, CA, USA). A back-to-back pair of angular contact bearings (S 626 C TA, GMN Bearing, Nuremberg, Germany) are press fit onto the screw, which is then inserted into the bearing housing during assembly. The inner race of the bearings is preloaded between the bearing adapter and the custom shaft coupling, and the outer race is preloaded between the actuator housing and the bearing housing. The base of the nut is secured to the foot plate through a U-joint connection, preventing rotation of the nut and constraining the rotation of the motor to produce linear translation of the actuators.

The linear actuators interface with the system via U-joint attachment points on the foot plate and mounting bracket. The U-joint attachment between the actuator nut and the foot plate prevents the nut from rotating, which forces linear extension and contraction without the need of a linear slide mechanism.

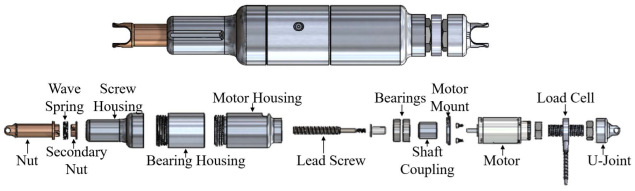

Fig. 5. Custom linear actuator design. Non-backdrivable linear actuator design, exploded view shows all components; U-joint attachment, load cell, motor housing, brushed DC motor, motor mount, shaft coupler, bearing housing, angular contact bearings, bearing adapter, ACME lead screw, actuator hosing, anti-backlash nut, wave spring, nut.

A secondary anti-backlash nut is preloaded against the primary nut, compressing a wave spring (CMS14-M1, Smalley, Lake Zurich, Il, USA), which decreases backlash in the system when it changes direction of travel. A load cell is mounted in line with each actuator, allowing for accurate sensing of ankle torque. The proximal end of each actuator is attached to a mounting bracket that clamps onto the endoskeletal support pylon. The motor housing, bearing housing, and actuator housing have threads machined into the interface and screw together during actuator assembly. The motor bolts onto the motor mount plate via the bolt pattern in the motor's face. This motor mount has flanges that interface with slots on the motor housing, which is compressed between the motor housing and bearing housing during assembly, preventing rotation of the motor.

The U-joint attachment, motor housing, motor mount, bearing housing, and actuator housing are precision machined from 7075T6 aluminum. The lead screw and bearing adapter are machined from alloy steel. The anti-backlash nut and primary nut are machined from 544 bearing bronze to reduce friction in the transmission. The non-backdrivable actuator design allows for high static holding torque without the need of a high-power motor or clutch.

B. Electronics Design

1) Embedded System: The prosthesis is controlled by a custom FlexSEA embedded system designed specifically for wearable robotic applications [22]. The custom embedded system (FlexSEA Pocket, Dephy Inc., Maynard, MA, USA) has integrated motor controllers, power management, and a microcontroller (STM32F405RGT6, STMicroelectronics, Geneva, Switzerland). The motor controller is programmed using the C programming language. The board is Bluetooth enabled for real-time monitoring of sensor values and the control loop.

2) Motor Selection: A brushed DC motor (DCX 22S, Maxon Group, Sachseln, Switzerland) was selected for the actuator design based on the torque and velocity requirements. The motor was selected for being able to provide the required ankle torque output of 1 Nm, and to minimize the actuator length. The selected motor has graphite brushes, ball bearings, and an integrated optical encoder.

3) Sensors:

a) Load cell: A load cell (LCM200, Futek Advanced Sensor Technology, Inc., Irvine, CA, USA) is integrated axially in each actuator, in order to provide accurate torque sensing

about the ankle-foot joint. This load cell has a nominal voltage output of 2 mV/V, with non-linearity of ±0.5% of the rated output.

b) Motor encoder: The motor encoder (ENX16 EASY 512IMP, Maxon Group, Sachseln, Switzerland) is a quadrature incremental optical encoder with 512 counts per turn. The encoder is used to send motor position state to the embedded system. The encoder operates from a supply voltage of 5 V and has a standstill current draw of 23 mA.

c) Lithium polymer battery: The actuators, EMG system, and embedded system are powered by a single 3 cell lithium polymer battery with a capacity of 800 mAh (T800.3S.30, Turnigy, Kwun Tong, Hong Kong).

C. EMG Acquisition and Processing

Muscle activation values from two pairs of agonist/antagonist muscles in the residual limb are measured and used to control the prosthesis output in real-time. The tibialis anterior (TA) and lateral gastrocnemius (LG) control dorsi- and plantar flexion, respectively, and the tibialis posterior (TP) and peroneus longus (PL) control inversion and eversion, respectively. As discussed in Section IV-A, the subject is a recipient of a novel amputation procedure called the agonist-antagonist myoneural interface (AMI). This procedure creates two pairs of agonist-antagonist muscle segments, one composed of the TP and PL, and the other composed of the TA and LG [23]. This procedure relocates the TP such that the muscle activation signal is accessible via surface electrodes [23]. A previous work by some of the authors developed a portable EMG acquisition and processing platform for active lower-extremity prosthetic system research [24]. The developed platform consists of a custom designed prosthetic liner and an embedded electronic system. During the design of the custom EMG liner, standard surface EMG electrodes are first affixed to the skin of the subject, adjacent to each of the four muscles used for device control (TA, LG, TP and PL) to confirm that activation of each muscle resulted in the desired EMG signal. Subsequently, the standard prosthetic liner of the subject was donned over the electrodes, and their positions were marked on the liner. The liner was then scanned using a laser scanner (FastSCAN, Polhemus, Colchester, Vermont) and a 3D model of the liner including the 3D positions of each of the electrodes was constructed. Lastly, a custom liner with embedded dry fabric EMG electrodes was manufactured. The custom prosthetic liner (Ottobock, Inc., Duderstadt, Germany) contains 8 bipolar channels of dry fabric EMG electrodes, and the electrodes are physically accessible through an external electrical connector.

The embedded EMG electronic system acquires raw EMG signals from the residual limb through the electrical connector on the liner. The embedded system amplifies and digitizes the raw signals, processes the signals with a bandwidth filter of 1kHz on a microprocessor (STM32F405RGT6, STMicroelectronics, Geneva, Switzerland), and feeds the signal to the high-level controller on the prosthesis. The raw EMG signals are filtered with a band-pass filter of 80-420 Hz and averaged with a 100-ms windows. The processed EMG data is converted to percent maximum voluntary contraction (%MVC) based on MVC values collected during a calibration stage of the device prior to each session. During calibration, the subject is asked to perform a maximal contraction for 10 seconds for each of the four muscles used for device control, TA, LG, TP, and PL. The maximum voltage recorded during the calibration period for each muscle is used as %MVC in the control system. The embedded EMG system feeds the processed EMG data to the embedded system on the prosthesis via a I2C communication protocol with a bandwidth of 1 kHz [24]. Fig. 6 shows the portable EMG acquisition and processing platform installed on a custom-built socket. The portable EMG acquisition and processing platform allows for muscle signals from the residual limb to be measured in real time while the subject is moving.

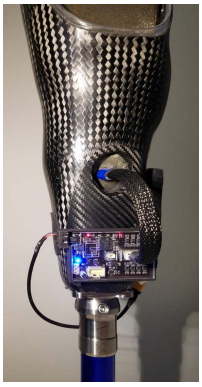

Fig. 6. The portable EMG acquisition and processing platform installed on a custom-built socket. The EMG board reads muscle activation signals from the custom liner, filters and processes the signal, and sends the processed signals to the embedded system.

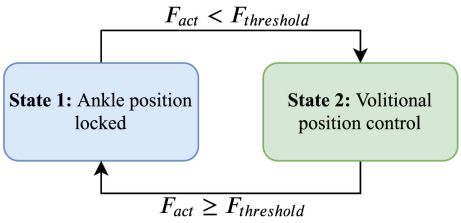

Fig. 7. High level finite-state machine includes two states: State 1 when the ankle-foot prosthesis is supporting body weight and the non-backdrivable transmission locks the ankle position in place, and State 2 when the ankle-foot prosthesis is in free space and neural inputs control position of the foot. Measured axial force (F_{act}) on the actuators is compared against a force threshold ($F_{threshold}$) of 10 N to trigger state transitions.

D. Control System Design

The high-level control system operates within two distinct states; when the device is supporting body weight of the user (State 1), and when the device is unloaded in free space (State 2) (Fig. 7). When load above the stance threshold (10 N) is detected on either of the actuators through the load cells, the actuators are turned off, locking the ankle position and withstanding up to 100 Nm of static torque (State 1). When the applied torque on the ankle is less than the threshold of the system, the actuators provide a maximum of 1 Nm of

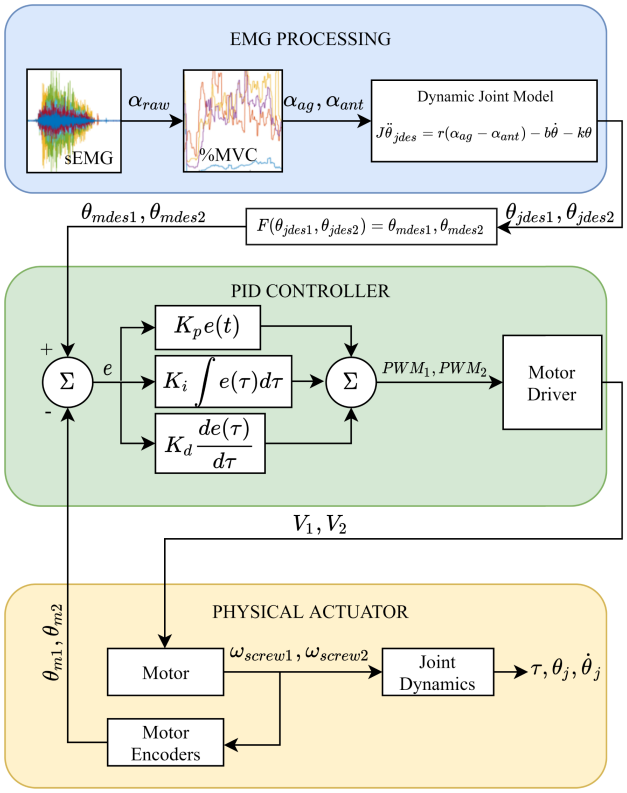

Fig. 8. Control system block diagram showing the three stages of processing; EMG processing, position control, and device output.

dynamic torque in order to re-position the foot according to neural inputs detected from the EMG system (State 2).

The control system has three stages: EMG processing, position control, and actuator output (Fig. 8). In the EMG processing stage, muscle activation values are recorded on the EMG system are filtered and then used as inputs for a virtual joint dynamic model. The virtual joint dynamic model calculates intended torque output for the virtual joint and uses that to calculate position and velocity of the robotic ankle. This position target is then fed into the position controller as a pulse width modulation (PWM) command.

1) Iterative Dynamic Joint Model: The iterative dynamic joint model is based off the control system developed by some of the authors in prior work [23], and converts muscle activation signals to desired device joint angle. This model interprets the EMG signal and converts it to desired prosthesis behavior, is described using the following equations [23]:

$$J\ddot{\theta} = \tau - b\dot{\theta} - k\theta \tag{1}$$

where J, b, and k are the inertia, damping, and stiffness characteristics of the virtual ankle-foot complex and τ is the torque about the virtual joint.

$$\theta_{des} = \iint \ddot{\theta} = \iint \frac{1}{J}\left(r\alpha_{ag} - r\alpha_{ant} - b\dot{\theta} - k\theta\right) \tag{2}$$

For each joint (ankle and subtalar), α_{ag} and α_{ant} are the EMG activation levels of the agonist and antagonist muscles normalized to %MVC, r is the moment arm of the virtual ankle joint, θ, $\dot{\theta}$, and $\ddot{\theta}$ are the position, velocity, and acceleration of the virtual joint, and θ_{jdes} is the desired joint position of the physical prosthesis. The moment arm for each muscle is determined based on the insertion point of each muscle in a biological joint and is hand tuned during calibration of the device [25].

This model uses muscle activation levels to estimate intended agonist and antagonist muscle force, and uses this to calculate intended torque about the virtual joint. This torque value is applied to a dynamic model of the ankle-foot prosthesis, outputting a target joint angle for each DOF. The target angles are sent to the position controller in the next stage of the control system.

2) Position Controller: The position controller receives desired joint angle commands from the dynamic joint model, feeds these commands to a proportional-integral-derivative (PID) controller on the embedded system, and sends a pulse width modulation (PWM) signal to each actuator. Sensor feedback is sent from the motor encoders in each actuator, as well as the load cells.

TABLE II
ANKLE-FOOT PROSTHESIS MASS DISTRIBUTION

Component	Mass (g)	Quantity
Climbing foot	339	1
Lithium Polymer battery	78	1
Motor	66	2
Pyramid adapter	60	1
Pylon	57	1
Ankle joint	59	1
Bracket	52	1
Motor Housing	41	2
Foot plate	32	1
Bearing housing	30	2
Electronics housing	29	1
Nut	27	2
FlexSEA embedded system	22	1
Actuator housing	19	2
Futek LCM200	17	2
Protective shell	16	1
Lead screw	9	2
Load cell attachment	7	2
Angular contact bearing	7	4
Heat sink	7	1
Shaft coupler	5	2
Antibacklash nut	2	2
Motor mount	2	2
Bearing sleeve	0.3	2
Wave spring	0.7	2
Hardware	62.5	-
Total	**1292**	

III. DEVICE VALIDATION

The final ankle-foot prosthesis prototype was evaluated to determine if the device meets the design requirements. The achieved values for the device specifications are presented in Table I.

A. Mechanical Design Validation

1) Mass: The mass distribution of the final system is outlined in table II. The total mass is 1292 grams, which meets the design requirement for device mass.

2) Range of Motion: Another important design requirement is the range of motion of the system. Range of motion of the

TABLE III
STATE, POWER CONSUMPTION, AND TORQUE DURING EACH OF THE 2 STATES IN THE FINITE STATE MACHINE

State	Functionality	Power	Torque
1	Ankle position locked	0.5 W	100 Nm (static)
2	Volitional position control	15.5 W	0.55 Nm (dynamic)

system was validated though bench-top testing by commanding the device through full range of motion of the actuators, and recording the actuator lengths at each position. Actuator encoder values were then converted to joint angles using the process described in section IV-B. The measured range of motion of the final system is 0.29 radians of dorsiflexion, −0.29 radians plantar flexion, 0.39 radians eversion, and −0.39 radians inversion.

3) Structural Stiffness: Structural stiffness of the system was evaluated to ensure that total deflection of the device when loaded with body mass was minimal. Geometric errors due to backlash in the lead screws and clearance in the u-joint connections result in an estimated 0.007 radians angular deflection of the foot. Worst case expected load-induced errors were calculated based on the stiffness of components along the structural loop, with an expected worst-case angular deflection of 0.034 radians.

B. Electronics Validation

The performance of the electronics was verified by measuring motor current and motor voltage while moving the device at a speed of 1 radian/second. The peak current is 3.2 amps during dorsiflexion and 3.0 amps during plantar flexion. Peak power is 15.5 watts, and power consumption of the electronics while the motors are not being driven is approximately 0.5 Watts. Table III outlines the power consumption and torque production in each state.

C. Control System Validation

The actuator step response and accuracy were validated through bench-top testing to validate the position controller and to confirm that the system meets the design requirements. This evaluation includes the PID controller and Physical Actuator blocks of the control diagram shown in Fig. 8. As the iterative dynamic joint model was initially used in previous research [23], the control loop from muscle activation to desired joint output were assumed to be valid based on previous validation of this control architecture, and was not specifically analyzed in this experiment. During this test, a joint angle position command was sent to the prosthesis at a frequency of $\frac{1}{3}$ Hz in increments of 0.09 radians throughout the device range of motion. Motor encoder data was logged at a frequency of 250 Hz from the embedded system. Fig. 9 shows the position command target (gray) and the actuator response (blue). The ankle joint of the prosthesis reaches 95% of the target value in approximately 120 milliseconds. The speed of the step response is approximately 2.18 radians/second.The accuracy of the system is 0.008 radians. This response time, joint velocity, and accuracy meet the design requirements listed in Table I.

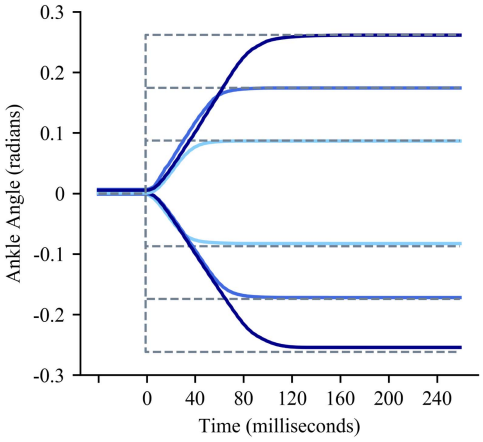

Fig. 9. Step response of ankle-foot prosthesis. Dashed lines are position target, blue lines are device position. The ankle joint moves at a joint velocity of 2.18 radians/seconds with a settling time of 120 milliseconds. The steady state error of the system is 0.008 radians.

IV. HUMAN SUBJECT EVALUATION

A preliminary human subject evaluation was conducted to evaluate the effect of the device on rock climbing performance. A subject with a unilateral transtibial amputation performed rock climbing routes with his traditional passive rock climbing prosthesis and with the presented robotic device.

A. Experimental Design

This study was approved by the MIT Committee on the Use of Humans as Experimental Subjects (protocol number: 1609692618A010, approval date: November 1, 2018), and written informed consent was obtained.

The participant with transtibial amputation (height: 172 cm, body mass: 75 kg, age: 52 years, gender: male, time since amputation: 28 months) is a trained, elite rock climber. The participant spent approximately seven hours training with the device prior to evaluation. The training protocol included approximately 4 hours of bench top training sessions during which the subject practiced using muscle activation to control joint positions of the robotic prosthesis. Training also included approximately 3 hours of climbing with the device while using EMG control before data was collected for the present study. The subject has also participated in experimental studies before in which he practiced using muscle activation to control device output [23]. The subject used a pin lock suspension mechanism with a silicone liner. The same socket and liner was used for both the passive and active trials. The subject is a recipient of the agonist-antagonist myoneural interface amputation, with demonstrated improved efferent prosthetic control [23]. The EMG system calibration was performed before starting the trials and once every hour to account for muscle fatigue and any change in voltage signals due to changing humidity or shifting of the liner. During the

Fig. 10. The passive climbing prosthesis used for the study is a custom made carbon fiber, wood, and rubber prosthesis that is the preferred climbing prosthesis of the study participant.

climbing session, knee and hip joint angles were recorded using a wearable goniometer system (DATALite, Biometrics Ltd., Newport, UK), and ankle and subtalar joint angles and torques were recorded from sensors on-board the robotic prosthesis. The knee and hip goniometers were attached to the subject on the lateral side of the left leg, affixed with medical tape. The goniometers remained mounted in the same position throughout all trials. Goniometer calibration was performed by recording sensor readings of the subject while standing in a neutral position, and was repeated ever hour. EMG data from the EMG board was recorded on the embedded system. Axial force on each actuator is recorded from the inline load cells. Ten trials for each condition (passive and robotic) of a selected route in a climbing gym (Brooklyn Boulders, Somerville, MA) were used for evaluation. The route was selected difficulty level in the mid-range of the subject's ability (5.10a) and variety of types of moves required. The subject was asked to climb the first 20 feet of the selected route. The subject used the same hold and same moves during each trial. The selected route did not include dynamic climbing moves. Video was recorded to synchronize the recorded data with each move on the route. The experiments were performed with the robotic prosthesis as well as a passive prosthesis, in sets of 5 trials each in a random order. The passive prosthesis used for comparison is a passive prosthesis constructed of wood, carbon fiber, and rubber, with a mass of 635 grams (Fig. 10). This prosthesis was custom made by the subject and was used for the experiment because it is the subject's preferred prosthesis for climbing.

B. Data Analysis

The recorded video was manually segmented for each climbing move. The first 3 moves of each trial were used for data analysis. The joint angle data for the knee and hip was extracted from the goniometer system, synchronized using video data, and segmented.

1) Motor Encoder to Joint Angle: In order to convert the motor encoder readings to joint angles of the device, first the inverse kinematics of the system were solved to determine the required lengths of each actuator for a given ankle and subtalar angle using Euler rotation matrices. Rotation matrices for the ankle and subtalar joints are as follows:

$$R_x(\theta_{ank}) = \begin{pmatrix} 1 & 0 & 0 \\ 0 & cos(\theta_{ank}) & -sin(\theta_{ank}) \\ 0 & sin(\theta_{ank}) & cos(\theta_{ank}) \end{pmatrix} \quad (3)$$

$$R_y(\theta_{sub}) = \begin{pmatrix} cos(\theta_{sub}) & 0 & sin(\theta_{sub}) \\ 0 & 1 & 0 \\ -sin(\theta_{sub}) & 0 & cos(\theta_{sub}) \end{pmatrix} \quad (4)$$

The overall rotation about the prosthesis joint is described by the following equation:

$$R = R_x(\theta_{ank}) * R_y(\theta_{sub}) * I \quad (5)$$

This rotation matrix is then used to calculate the required length of each actuator for a given ankle and subtalar angle by the following equation:

$$L_i = h + R * r_i - d_i \quad (6)$$

where L_i is the length of the actuator, h is the distance between the rotating reference frame attached to the foot (X', Y', Z') and the prosthesis reference frame (X, Y, Z), r_i is the actuator distal mounting location, and d_i is the proximal actuator anchor point.

In order solve the forward kinematics to convert the actuator encoder positions to joint angles, a system of equations comprising of Eq. 6 for each actuator is solved numerically for the two unknown joint angles (θ_{ank} and θ_{sub}) using MATLAB (MATLAB R2018b, Mathworks, Natick, MA).

2) Joint Torque Calculations: Joint torque is calculated from the axial force measurements using the following equation:

$$\tau_{total} = \vec{F}_0 \times \vec{r}_0 + \vec{F}_1 \times \vec{r}_1 \quad (7)$$

where F_0 and F_1 are the axial forces on the left and right actuators, and r_0 and r_1 are the moment arms between the ankle joint the the lower actuator attachments (Fig. 11). The torque about the ankle joint axis is calculated as:

$$\tau_{ankle} = \tau_{total} \cdot \hat{e'}_x \quad (8)$$

where $\hat{e'}_x$ is the unit vector in the direction of the x axis, and the torque about the subtalar joint axis is calculated as:

$$\tau_{subtalar} = \tau_{total} \cdot \hat{e'}_y \quad (9)$$

where $\hat{e'}_y$ is the unit vector in the direction of the y axis.

V. Results

Ankle, knee, and hip joint angles for the test subject during three moves on the climbing wall are shown in Fig. 12. Average joint angles from the 10 trials of each condition are shown for the active prosthesis (blue) and the passive prosthesis (gray). Standard deviation is shown by the shading. The maximum plantar flexion achieved with the robotic prosthesis is -0.25 radians, and maximum dorsiflexion is 0.07 radians. Maximum plantar flexion and dorsiflexion for

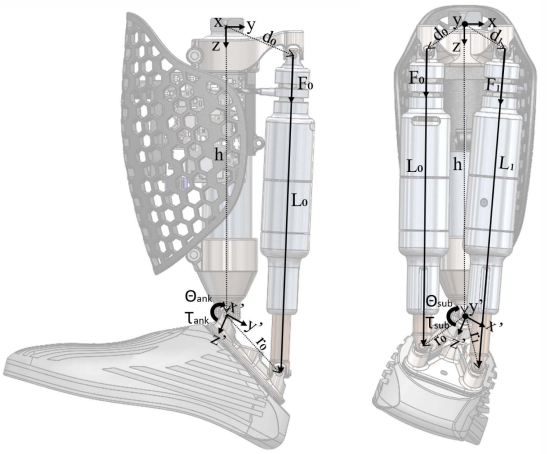

Fig. 11. Joint angles, coordinate systems, force vectors, and position vectors used for torque calculations and inverse kinematics calculations. F_i is the axial force on each actuator, L_i is the length of each actuator, r_i is the actuator distal mounting location, d_i is the proximal actuator anchor point, (X, Y, Z) is the non-rotating prosthesis reference frame, (X', Y', Z') is the rotating reference frame attached to the foot, h is the distance between the two reference frames, τ_{ank} and τ_{sub} are the torques about the ankle and subtalar joints, and θ_{ank} and θ_{sub} are the ankle and subtalar joint angles.

the passive device are 0 radians. Maximum eversion with the robotic prosthesis is 0.007 radians, maximum inversion is −0.08 radians. The passive prosthesis has a maximum inversion and eversion of 0 radians. Knee angle also differs between the active prosthesis trials and passive prosthesis trials. Maximum knee flexion is lower while climbing with the powered prosthesis, −0.69 radians compared to −1.06 radians with the passive prosthesis. Hip flexion while climbing with the robotic prosthesis reaches a maximum of 0.97 radians, compared to a maximum of 1.11 radians with the passive prosthesis.

Representative data from a single trial is plotted in Fig. 13 showing EMG activity, joint angles, load cell force, and joint torque. EMG activity is normalized based on %MVC. The gray regions indicate the periods of time when the axial force on the actuators is greater than the 10 N threshold, and the non-backdrivable transmission locks the ankle in place.

VI. Discussion

In this article, we described the design, validation, and clinical evaluation of a 2-DOF EMG-controlled ankle-foot prosthesis with a non-backdriveable transmission. The device validation shows that the prosthesis successfully achieves targeted device mass, range of motion, torque output, joint velocity, accuracy, build height, and battery life. The mass of the robotic prosthesis compares favorably to the powered and quasi-passive devices discussed in Section I. The prosthesis characterization verified that the position command response time of the prosthesis has sufficient accuracy and speed.

The clinical evaluation validated the performance of the ankle-foot prosthesis during rock climbing, and provided preliminary evidence for the potential advantages of a EMG controlled 2-DOF prosthesis during climbing. Results from the preliminary human subject testing demonstrate that the

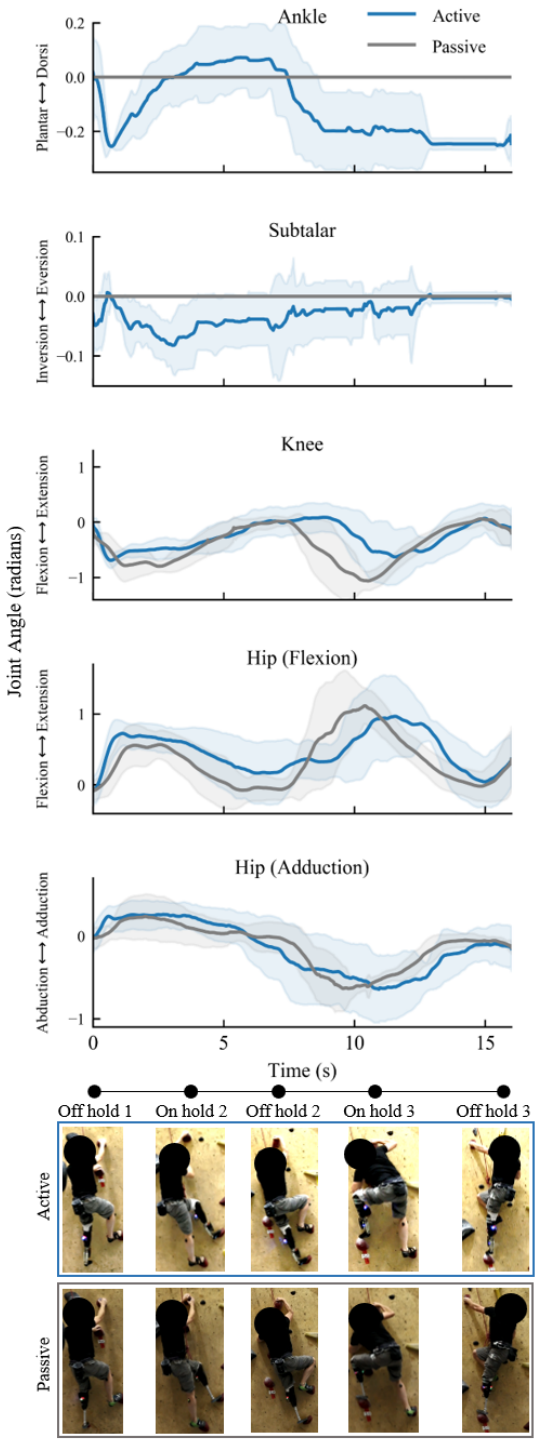

Fig. 12. Joint angles with passive prosthesis and powered prosthesis. Joint angles of the ankle, knee, and hip during rock climbing with the passive prosthesis (gray), and the powered prosthesis (blue). The trials are averaged and the standard deviation is shown in shading.

subject with transtibial amputation utilizes both DOF of the rock climbing prosthesis while climbing (Fig. 12). The range of motion of the ankle joint while climbing with the robotic prosthesis was 0.31 radians, compared to 0 radians with the passive prosthesis. The subtalar joint range of motion was 0.09 radians with the robotic device, compared to 0 with the

passive prosthesis. This indicates that the subject is able to manipulate the position of the prosthesis in real time while rock climbing, utilizing both DOF of the device to expand range of motion over the passive device. During evaluation on the selected route, the full range of motion of the robotic prosthesis was not utilized. Further testing on a variety of climbing routes with additional subjects is needed to determine utility of the full range of motion.

The maximum hip flexion and knee flexion angles while climbing with the robotic prosthesis are lower than with the passive prosthesis (Fig. 12). The rate of change of hip angles and knee angles is also lower than with the passive device. This result could be due to the increased range of motion of the robotic prosthesis, which leads to less required excursion of the knee and hip while climbing. Further work is necessary to determine the significance of these results. Fig. 13 demonstrates the device's ability to interpret EMG activity from the residual limb, and convert that data into intended joint position in real time. This validates the performance of the system during rock climbing.

Subject testimonial during the study provided positive feedback on the effect of the robotic prosthesis. The subject indicated that the control of the device felt intuitive and sufficiently fast during rock climbing. He said that by adjusting the joint angle of the device he felt he was able to more accurately position his foot on the holds. The subject also mentioned that due to his adjustment of the foot position while climbing, the loading of the prosthetic socket felt more comfortable. Research has shown that optimal prosthesis alignment can improve the comfort and function of the prosthetic socket by altering the force and moment induced by the prosthesis [26]. Decreasing moments on the prosthesis socket is another potential benefit of this device that should be explored further in future work by directly measuring moments and forces at the socket interface.

Further studies are needed to assess the clinical efficacy of the prosthesis on a larger subject population. Additional biomechanical studies will be performed with a larger number of subjects to further explore the benefits that the device has on the biomechanics of people with transtibial amputation. Human subject data will be collected using full body motion capture to analyze the effect of the robotic prosthesis compared to a passive device with a larger number of subjects. Biomechanics will also be compared to climbing technique of people with intact biological limbs. The device will be tested while climbing on a wider variety of routes to determine what types of rock climbing moves the robotic ankle-foot prosthesis provides the most benefit for.

Future designs of the ankle-foot prosthesis could improve upon the current system. Mass of the system could be reduced by changing the size or the material of the climbing foot, as it is currently the component with the largest mass. The mass could be further reduced by using a battery with a lower electric charge rating. The 800 mAh battery used in the device has lasted approximately 4 hours on a single charge during human subject testing, which exceeds our functional requirement of 2 hours. Future designs will decrease build height of the device to allow for people of more sizes and amputation levels to use the device. In addition, the response time of the actuators could be further reduced by decreasing control system delays or increasing the power of the motors.

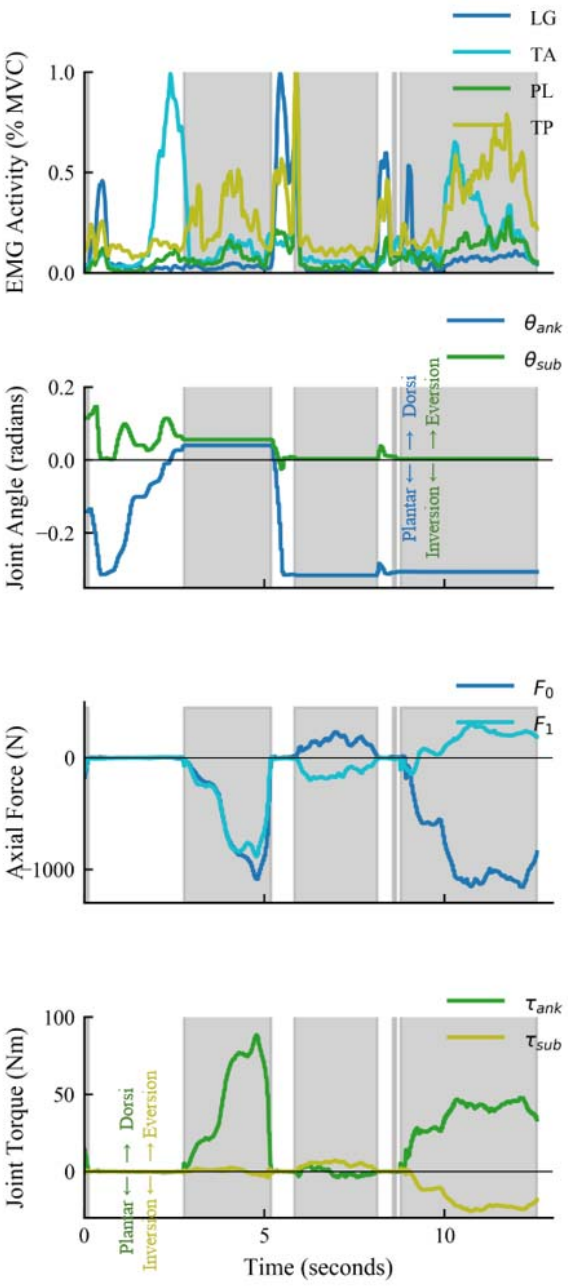

Fig. 13. EMG activity, joint angles, load cell force, and joint torque. EMG activity is recorded during climbing and converted to intended device output through the iterative dynamic joint model. Gray regions indicate periods of time when axial force on actuators is greater than the force threshold.

VII. Conclusion

In this article, we present the first 2-DOF EMG-controlled robotic transtibial prosthesis. In addition, this is the first robotic prosthesis designed specifically for rock climbing. This ankle-foot prosthesis uses a novel non-backdrivable actuator approach to achieve more actuated DOFs in a lower mass

package than all existing powered prostheses. This device increases ankle and subtalar range of motion during rock climbing compared to a passive rock climbing prosthesis. This article presents initial results showing potential benefits of such a device on the biomechanics of a person with transtibial amputation while rock climbing. The prosthesis technology presented in this article has broad applications and could potentially benefit any form of locomotion where actuated DOFs are desired, a light weight device is necessary, and no dynamic torque generation during stance is required. This technology could be used for terrain adaptation during hiking, safer stair ascent and descent during daily life, and swing phase toe clearance during walking. This technology has the potential to increase accessibility of physical activity for people with amputation, helping improve physical and mental health as well as quality of life.

Acknowledgment

The authors would like to thank Bob Emerson at A Step Ahead Prosthetics for the fabrication of the custom prosthetic socket, and J. F. Duval at Dephy for the design and programming of the FlexSEA embedded system. *Author Contributions:* E.A.R contributed to conceptualization of the device design, performed the mechanical and electronic design, assembled the prosthesis, programmed the prosthesis, designed the experiments, collected, processed, and analyzed data, and wrote the manuscript. M.E.C. contributed to the mechanical design, and provided feedback on the manuscript. S.H.Y. designed and programmed the EMG embedded system, contributed to programming the prosthesis, and assisted with data collection. T.R.C. developed the iterative dynamic joint model and assisted with data collection. D.S. designed the custom socket liner and provided feedback on the manuscript. H.M.H. conceived the device architecture, contributed to device design, controller design, experimental design, and writing of the manuscript.

References

[1] H. M. Herr and A. M. Grabowski, "Bionic ankle–foot prosthesis normalizes walking gait for persons with leg amputation," *Proc. Roy. Soc. B, Biol. Sci.*, vol. 279, no. 1728, pp. 457–464, Feb. 2012. [Online]. Available: https://www.ncbi.nlm.nih.gov/pmc/articles/PMC3234569/

[2] M. Couture, C. D. Caron, and J. Desrosiers, "Leisure activities following a lower limb amputation," *Disability Rehabil.*, vol. 32, no. 1, pp. 57–64, Jan. 2010.

[3] M. Bragaru, C. van Wilgen, J. Geertzen, S. Ruijs, P. Dijkstra, and R. Dekker, "Barriers and facilitators of participation in sports: A qualitative study on Dutch individuals with lower limb amputation," *PLoS ONE*, vol. 8, no. 3, pp. 1–9, Mar. 2013. [Online]. Available: http://dx.plos.org/10.1371/journal.pone.0059881

[4] A. J. De Luigi and R. A. Cooper, "Adaptive sports technology and biomechanics: Prosthetics," *PM R, J. Injury, Function, Rehabil.*, vol. 6, pp. S40–S57, Aug. 2014.

[5] Physical Activity Council. (2019). *2019 Physical Activity Council's Overview Report on US Participation*. [Online]. Available: http://www.physicalactivitycouncil.com/pdfs/current.pdf

[6] M. J. Highsmith, J. T. Kahle, J. L. Fox, K. L. Shaw, W. S. Quillen, and L. J. Mengelkoch, "Metabolic demands of rock climbing in transfemoral amputees," *Int. J. Sports Med.*, vol. 31, no. 01, pp. 38–43, Jan. 2010. [Online]. Available: http://www.thieme-connect.de/DOI/DOI?10.1055/s-0029-1239562

[7] C. J. Low, "Biomechanics of rock climbing technique," Ph.D. dissertation, School Sport Exercise Sciences, Univ. of Leeds, New Delhi, India, 2005.

[8] TRS Climbing. *El Dorado Z-Axis Foot*. Accessed: Nov. 19, 2019. [Online]. Available: https://www.trsprosthetics.com/product/climbing/

[9] Evolv Sports. *Evolv Adaptive Foot*. [Online]. Available: https://evolvsports.com/evolv-adaptive-foot-eaf/

[10] Mountain Orthotic & Prosthetic Services. *ADK Rock Climbing Foot*. [Online]. Available: http://www.mountainoandp.com/adkfoot/

[11] Ottobock. *USEmpower*. Accessed: Nov. 19, 2019. [Online]. Available: https://www.ottobockus.com/prosthetics/lower-limb-prosthetics/solution-overview/empower-ankle/

[12] S. K. Au, J. Weber, and H. Herr, "Powered ankle-foot prosthesis improves walking metabolic economy," *IEEE Trans. Robot.*, vol. 25, no. 1, pp. 51–66, Feb. 2009. [Online]. Available: http://ieeexplore.ieee.org/document/4738392/

[13] E. M. Ficanha, G. A. Ribeiro, H. Dallali, and M. Rastgaar, "Design and preliminary evaluation of a two DOFs cable-driven ankle–foot prosthesis with active dorsiflexion–plantarflexion and inversion–eversion," *Frontiers Bioeng. Biotechnol.*, vol. 4, p. 36, May 2016. [Online]. Available: https://www.ncbi.nlm.nih.gov/pmc/articles/PMC4852183/

[14] Ossur. *Proprio Foot*. Accessed: Nov. 19, 2019. [Online]. Available: https://www.ossur.com/en-us/prosthetics/feet/proprio-foot

[15] M. Alimusaj, L. Fradet, F. Braatz, H. J. Gerner, and S. I. Wolf, "Kinematics and kinetics with an adaptive ankle foot system during stair ambulation of transtibial amputees," *Gait Posture*, vol. 30, no. 3, pp. 356–363, Oct. 2009.

[16] R. D. Bellman, M. A. Holgate, and T. G. Sugar, "SPARKy 3: Design of an active robotic ankle prosthesis with two actuated degrees of freedom using regenerative kinetics," in *Proc. 2nd IEEE RAS EMBS Int. Conf. Biomed. Robot. Biomechatronics*, Oct. 2008, pp. 511–516. [Online]. Available: http://ieeexplore.ieee.org/document/4762887/

[17] T. Lenzi, M. Cempini, J. Newkirk, L. J. Hargrove, and T. A. Kuiken, "A lightweight robotic ankle prosthesis with non-backdrivable cam-based transmission," in *Proc. Int. Conf. Rehabil. Robot. (ICORR)*, Jul. 2017, pp. 1142–1147.

[18] A. Tilley, *The Measure of a Man and Woman: Human Factors in Design*. New York, NY, USA: Henry Dreyfuss Associates, 1993.

[19] D. Winter, "Anthropometry," in *Biomechanics and Motor Control of Human Gait: Normal, Elderly And Pathological*, 4th ed. Hoboken, NJ, USA: Wiley, 2009, pp. 82–106. [Online]. Available: https://trid.trb.org/view.aspx?id=770965

[20] Department of Heath and Human Services. (Aug. 2016). *Vital and Health Statistics. Series 3, Data From The National Health and Nutrition Examination Survey*. [Online]. Available: https://stacks.cdc.gov/view/cdc/40572

[21] A. Roaas and G. B. J. Andersson, "Normal range of motion of the hip, knee and ankle joints in male subjects, 30–40 years of age," *Acta Orthopaedica Scandinavica*, vol. 53, no. 2, pp. 205–208, Jan. 1982. [Online]. Available: http://www.tandfonline.com/doi/full/10.3109/17453678208992202

[22] J.-F. Duval and H. M. Herr, "FlexSEA: Flexible, scalable electronics architecture for wearable robotic applications," in *Proc. 6th IEEE Int. Conf. Biomed. Robot. Biomechatronics (BioRob)*. Singapore: IEEE, Jun. 2016, pp. 1236–1241. [Online]. Available: http://ieeexplore.ieee.org/document/7523800/

[23] T. Clites *et al.*, "Proprioception from a neurally controlled lower-extremity prosthesis," *Sci. Transl. Med.*, vol. 10, no. 443, pp. 1–13, May 2018. [Online]. Available: http://stm.sciencemag.org/content/10/443/eaap8373

[24] S. Yeon, "Design of an advanced sEMG processor for wearable robotics applications," M.S. thesis, Massachusetts Inst. Technol., Cambridge, MA, USA, Sep. 2019.

[25] P. Klein, S. Mattys, and M. Rooze, "Moment arm length variations of selected muscles acting on talocrural and subtalar joints during movement: An *in vitro* study," *J. Biomechanics*, vol. 29, no. 1, pp. 21–30, Jan. 1996.

[26] T. Kobayashi, T. G. Rosenbaum-Chou, M. S. Orendurff, D. A. Boone, and A. K. Arabian, "Effect of prosthetic alignment changes on socket reaction moment impulse during walking in transtibial amputees," *J. Biomechanics*, vol. 47, no. 6, pp. 1315–1323, Apr. 2014. [Online]. Available: https://www.ncbi.nlm.nih.gov/pmc/articles/PMC3997505/